Passive ground-based optical techniques for monitoring the on-orbit ICESat-2 altimeter geolocation and footprint diameter

Lori A. Magruder[1], Kelly Brunt[2,3], Thomas Neumann[2], Bradley Klotz[1], and Michael Alonzo[1]

[1]Applied Research Laboratories, University of Texas at Austin, Austin, TX.

[2] NASA Goddard Space Flight Center, Greenbelt, MD

[3] University of Maryland College Park, College Park, MD

Corresponding author: Lori A. Magruder[†] (magruder@arlut.utexas.edu)

[†] Address: 10000 Burnet Rd., Austin, TX, 78758.

Key Points:

- Corner cube retro-reflectors are passive optical components that provide a distinct and recognizable reflection signature to space-based lidar for validation of the measurement geolocation.
- The passive optics also provide a methodology for determining the diameter of the laser footprint on the surface and the effects of the atmospheric attenuation on the effective spot size.
- Validation studies confirm that the accuracy ICESat-2 geolocation at both mid-latitude and polar regions currently meet the mission requirement for position quality.

Plain Language Summary

NASA launched its second Earth observing laser altimeter in 2018 with mission objectives of studying the changes in our climate by monitoring global elevations, particularly in the polar regions. Since the mission is focused on generating accurate elevations and elevation change, the geolocation (or geodetic position) of the measurements are of upmost importance to each of the scientific disciplines supported by these observations. Geolocation validation is required to ensure that the mission is meeting its objectives with the appropriate level of geolocation accuracy. One validation technique uses small optical reflectors placed in a specific pattern along one or more satellite ground-tracks. The optics provide a unique signal back to the satellite that can be used to compare the geolocation of these returns in the data to the known position on the surface. Results of the position comparison indicate the measurement locations are accurate to within 3.5 m with a standard deviation of 1.6 m. They also provide a method for determining a representative footprint diameter using geometric analysis, which resulted in an average value of 10.9 m ±2.1 m.

Abstract

Corner cube retro-reflectors (CCRs) are passive optical components that were used to independently evaluate the ICESat-2 laser altimeter geolocation and laser footprint diameter. These campaigns were performed in both mid-latitude and polar regions over the first 18 months of the mission. A proven technique using CCRs to evaluate the original ICESat mission was optimized for the ICESat-2 mission and deployed at White Sands Missile Range and along the 88º S line of latitude to passively monitor the geolocation accuracy, and estimate the diameter of the laser footprint. The results reveal an average geolocation accuracy of the ICESat-2 measurements to within 3.5 m ±2.1 m, meeting the mission requirement of 6.5 m. Additionally, the CCR evaluation of the footprint diameter resulted in 10.9 m ± 1.3 m, with the variability explained primarily through the influence of atmospheric conditions.

1. Introduction

The Ice, Cloud and land Elevation Satellite-2 (ICESat-2) is a NASA Earth observing satellite, on-orbit since September 2018. The motivation behind the mission is focused on observations over the polar regions to support ice-sheet elevation change and sea ice characterization studies. The observations are realized through ATLAS (Advanced Topographic Laser Altimeter System), a lidar instrument designed to provide precise ranging measurements of individual, 532 nm laser photon reflections from the surface of the Earth. These ranging measurements, combined with the satellite observatory position and laser pointing determination create a capability to quantify centimeter-scale elevation change over the ice sheets and sea ice freeboard (Neumann et al., 2019). ATLAS uses a single laser to provide 6 altimeter beams at 10 kHz. The beams are configured into 3 beam pairs with pairs spaced by ~3.3 km across track (Markus et al., 2017). Within each pair the spots are separated in the along-track direction by 2.5 km and 90 m in the across-track direction. Additionally, the pairs provide two distinct energy levels with the ‘strong’ spot at 4 times the level of the ‘weak’. The locations of the weak/strong spots in the 6 beam pattern is dependent on the orientation of the observatory relative to the direction of motion.

The mission requirements on satellite position and pointing determination ensure that the observations accurately support the mission science objectives with respect to geolocation.

Precision orbit determination (POD) is required to be within 5 cm radial accuracy while the precision pointing determination (PPD) requires laser pointing knowledge to within 3.7 μrad of precision, resulting in a total measurement geolocation knowledge of 6.5 m, or ~2.7 arc sec. The PPD solution quality is dependent on the ability to resolve the influence of thermal variations and spacecraft orientation on the pointing efficacy (Luthcke et al., 2019). Pointing corrections on-orbit are determined using a regular sequence of maneuvers over the ocean ('ocean scans') and within a full orbit ('around the world scans') to recover the range residuals and biases (Luthcke, et al., 2005). These calibrations are applied to the PPD to reach the pointing accuracy to support the mission geolocation requirement. Methods for validating the geolocation utilize comparison to ground reference surfaces, derived independently with high resolution airborne lidar (Magruder et al., 2020) or ground based GPS surveys (Brunt et al., 2019) to determine the vertical and horizontal accuracy of the ICESat-2 geodetic position.

A unique, independent method for geolocation accuracy assessment relies on small optical components, corner cube retroreflectors (CCRs). CCRs are designed to reflect light along the angle of incidence with diffraction properties dependent on the CCR diameter and energy wavelength (Sun et al., 2019). As such, careful selection of diameter allows the ground-based optics to return observable reflections to a space-based receiver (Magruder et al., 2020). These CCR signatures are distinct from the surface returns at the measurement rate, meaning no post-processing or aggregation is necessary to identify the presence of reflections from the optics within the data. Comparing the satellite measurement geolocation to the known geodetic position of the CCR gives the independent assessment of measurement positional accuracy. This technique was successful for ICESat (2003-2009; Magruder et al., 2005) and the airborne engineering testbed for ICESat-2, MABEL (Multi Altimeter Beam Experimental Lidar; Magruder and Brunt, 2018). Studies with MABEL determined the expected response of a CCR to photon-counting lidar and helped design the specific implementation details. The arrays placed at White Sands Missile Range (WSMR) utilized 8 mm diameter optics on poles with height variations from 0.6 m to 3 m in four arrays (Magruder et al., 2020a). CCR arrays placed along the 88º S (88S) line of latitude during a GNSS ground survey performed in 2017-2018 Antarctic summer season and revisited each year since use CCRs positioned where the satellite reference tracks (RGTs) spatially converge. The WSMR arrays are a diamond pattern with CCR arrays located at each of the vertices (north, south, east, and west). This pattern is capable of capturing a beam pair for both ascending and descending

tracks. For example, an ascending track could illuminate the east and north arrays with the right beam of a pair and the south and west array with the left beam of the pair. The design of the full ensemble at each CCR validation assumes the ICESat-2 satellite meets the pointing control requirement of ±45 m and the ability to maintain RGT tracking (Magruder et al., 2020b).

Here we present an evaluation of the ICESat-2 positional (horizontal geolocation) accuracy of the laser footprint and the estimation of the effective footprint diameter using all available CCR signature returns for the current mission lifetime (October 2018 – May 2020). Further, this study explores the variations in the results to radiometric effects due to the state of the atmosphere. The methods presented here provide an opportunity to passively monitor the performance of the satellite on-orbit. This method is critical to the continuous validation of ICESat-2, as it helps ensure that the scientific discoveries leveraging higher-level data products are based on accurate and precise low-level data.

2. Data and Methods

The CCR analysis focuses solely on the ICESat-2 Global Geolocated Photons (ATL03) data product. ATL03 is the Level 2a data product that provides the photon positional data in addition to many other parameters associated with uncertainties, corrections for tides and atmosphere and signal statistics (Neumann et al., 2019a). The ATL03 data used in this study are available through the National Snow and Ice Data Center (www.nsidc.org) and are part of the third release (r003) of final data products from the ICESat-2 Project Science Office (Neumann et al., 2019b). Since ATL03 includes photons associated with both surface reflections and solar background noise, the ATL03 processing algorithm also includes a filtering method that statistically delineates between the two. This is an important step particularly for the majority of the higher, Level 3a, products that rely on those photons identified with a high surface-signal probability to interpret the surface elevation (Smith et al., 2019, Kwok et al., 2019, Neuenschwander and Pitts, 2019).

The ICESat-2 reference ground-tracks (RGTs) create several opportunities to point ATLAS at the WSMR validation site using the up to 5 degree off-nadir pointing capability of the observatory. These 7 WSMR relevant RGTs equate to opportunities nearly twice a month over the course of the repeat ground-track cycle (91 days) and offer scenarios for both ascending and descending tracks. This variability in satellite direction of motion (northward or southward), combine with

possible orientation (forward or backward facing) and solar panel position to provide a comprehensive method for understanding the efficacy of the pointing calibration, the pointing control and overall geolocation knowledge of the satellite-based measurements under on-orbit conditions specific to a mid-latitude orbital position.

The CCR arrays deployed along the 88S line of latitude during a GPS traverse in the 2017-2018 Antarctic field season (Brunt et al., 2019) and resurveyed or relocated during the following two field seasons to optimize the opportunities for CCR illumination based on the results from the previous year. Given the 92^{o} orbit inclination, the ground tracks spatially converge at the extreme latitudes and provide a dense coverage of the region, allowing for many more CCR potential overpass opportunities than the WSMR location.

The analysis of the CCR signatures is described in Magruder et al. (2020a) and initiates with finding the elevated, linear signatures distinct from the estimated terrain surface in the relevant ATL03 transects. The second processing step extracts the CCR returns and generates a statistical estimate of along-track signal CCR length using the expected Gaussian energy distribution of the laser footprint. The laser footprint diameter is representative of a Gaussian beam diameter, as defined as the 2-sigma value of the signal distribution curve representative of 86% of the total beam energy based on pre-launch measurements of a Gaussian energy pattern (Martino et al., 2019). For a strong beam, the Gaussian beam energy value is 120 µJ while a weak beam provides 30 µJ (Neumann et al., 2019a). The CCR returns are quite pronounced but it is estimated that the spatial extent of the footprint size is susceptible to atmosphere attenuation or other optical loses. In this paper, we use the same statistically robust methodology of Magruder et al. (2020a) on the much larger set of CCR returns collected since that initial study. The chord length (e.g. the effective distance from leading edge to trailing edge of the initial illuminating footprint and final illuminating footprint respectively) is critical to understanding where the CCR is located relative to the center of the laser footprint diameter. Based on the ATL03 geolocation algorithm, the specific position of a reflector within the footprint dimeter is unresolvable as the geolocation for all of the surface-reflected photons for a given shot are geolocated to the laser footprint centroid (Luthcke et al., 2019). The CCR deterministic position within a laser footprint relies solely on its relative position to the footprint centerline that can be quantified by the length of the signal chord

length. This is more of an estimation when only one CCR is illuminated and the scenario lacks the geometric constraint for determining which side (east or west) of the footprint centerline the CCR is located. However, when two or more CCR signatures appear in a single transect, both the ATL03 geolocation accuracy and the Gaussian beam diameter can be determined. These estimations are derived using the known geometry of the CCR positions and the goodness of fit of the CCR signal signatures for a given beam diameter through an iterative process. By minimizing the horizontal residuals of the combined comparison over the sequence of CCR illuminations a quantitative assessment is achieved for the geolocation offsets in northing and easting that inform the accuracy of the horizontal position of the measurements.

Determination of geolocation accuracy and footprint diameter is dependent on the signal retrieval. Adequate signal retrieval implies that there is reasonable number of signal photons for accurate analysis given the retrieval technique. The number of signal photons depend on both the incident energy at the surface and returned energy at the receiver. The signal reflection strength is primarily dependent on the surface reflectance. However, atmospheric attenuation also is significant. Clouds, aerosols and water vapor in the atmospheric column attenuate the laser light through absorption and scattering. Initial predictions based on data prior to ICESat-2 launch suggested that column optical depth, a measure of the observed attenuation related to clouds and aerosols, could attenuate > 50% of the laser energy if the optical depth is above 1.0 (Palm et al. 2020).

To assess the atmospheric effects on the CCR geolocation validation and diameter retrievals, calibrated attenuated backscatter (CAB) and lower along-track-resolution parameters, including relative humidity, temperature, and pressure, are utilized from the ICESat-2 atmospheric product ATL09 (Palm et al., 2019). Specific humidity is determined from these variables following the computation of vapor pressure through the standard equations provided in Rogers and Yau (1996). The atmospheric profiles are separated into estimated boundary layer (surface – 1 km), low (1 km – 5 km), moderate (5 – 10 km), and high altitudes (10 – 15 km) to pinpoint specific levels where the moisture content is potentially high or where temperature inversions may trap scattering particles. For the cases at WSMR, the column optical depth and profile data are used to assess their effect on footprint diameter and associated geolocation accuracy. For those cases examined at 88S,

other parameters are considered from the atmosphere product, including the blowing snow confidence level which could cause additional attenuation through signal scattering. Moisture effects on the signal retrieval are more likely at WSMR than at 88S because temperatures are higher and the air can hold more water vapor. The depth of the troposphere at the mid-latitudes extends above 12 km height as well, especially during the summer months. For comparison, the tropospheric depth at 88S extends only to ~8 km before noticeable stratospheric warming begins. Therefore, the impact of the atmosphere will be different for the two locations based on these differences in atmospheric column characteristics.

3. On-orbit assessment 2019-2020

The first successful WSMR overpass in March 2019 captured the center weak beam on both the east and the north arrays. This initial analysis helped assess the geolocation of the ATL03 photons relative to the CCR positions for the first time and also helped establish the deterministic method for recovery of the footprint diameter (Magruder et al., 2020a). The result for this particular pass was a footprint diameter of 10.6 m and the ATL03 horizontal geolocation was accurate to within 2 m. This was an important discovery for several reasons that include: 1) the automation of the footprint diameter determination which proved to significantly impact the ability to retrieve the correct position of the CCR within the spatial extent of the illuminated areas; and 2) the realization of how the spacecraft pointing is implemented and executed in addition to understanding the constraints on the spacecraft pointing stability.

Favorable conditions in September 2019 allowed for the illumination of multiple CCRs with the center strong beam, during the second opportunity to explore the validation technique. The analysis of these signatures indicates a beam diameter of 12 m and horizontal geolocation offset of 5 m. The disparity in diameter recovered between the weak (March 2019) and strong (September 2019) beams, at the time, was attributed to atmosphere attenuation and potential loss of return signal at the edges of the footprint where the energy is lower (Magruder et al., 2020). Given the two instances of CCR signal retrievals, the concept and implementation were confirmed but the small sample size of data did not warrant statistically relevant conclusions for geolocation accuracy and beam diameter. As such, the pointing requests continued with regularity for the relevant RGTs within each full 91-day orbit cycle. Varied results were achieved at WSMR as some unsuccessful overpasses simply did not hit the CCR arrays while others were performed during

cloud cover that prevented returns from either the surface or the CCR. Other opportunities occurred coincident to anomalous satellite operational events which temporarily suspended on-orbit data collection. RGT #28, a descending pass on 28 March 2020 was particularly successful by illuminating 5 CCRs in both the north and east arrays after the satellite performed a roll maneuver to point ~4º off-nadir. Figure 1 (a – c) provides the configuration of the satellite ground track (ATL03 geolocated photons) and the array locations. In Figure 1 the signal photons attributed to the CCR returns are blue and the remaining ATL03 signal photons are green. Figure 1 (d-f) presents the along-track segments for three different CCRs that were illuminated. The heights of the individual signatures provide the initial identification of a specific CCR, as they were deployed with staggered heights with this consideration. In this case of Figure 1 (d-f), the sequential heights of 3 m, 0.75 m and 3 m, from North to South, is indicative of a CCR04, CCR08 and CCR12 illumination pattern. The identification of the CCRs in the east array is done similarly (CCR13 and CCR17). The signature chord length of each of the CCRs is statistically derived using a 2σ value from a Gaussian distribution of the extracted CCR signal. Using these chord lengths with the geometric constraints from the known CCR array positions results in a 12.0 m beam diameter and a horizontal geolocation offset of 4.3 meters (RMSE 2.1 m). The RMSE is representative of the goodness of fit of the predicted geolocation track to the 5 individual CCR positions. Figure 1 (g-h) illustrates the geolocation adjustment of the original track (black line) to accommodate the geometry of the known CCR locations (red X's) and the signal chord lengths (blue points) as an indicator of where the CCR is relative to the centerline of the laser footprint. The solution of the true positions (green points) allows the technique to estimate the accuracy of the ATL03 geolocation.

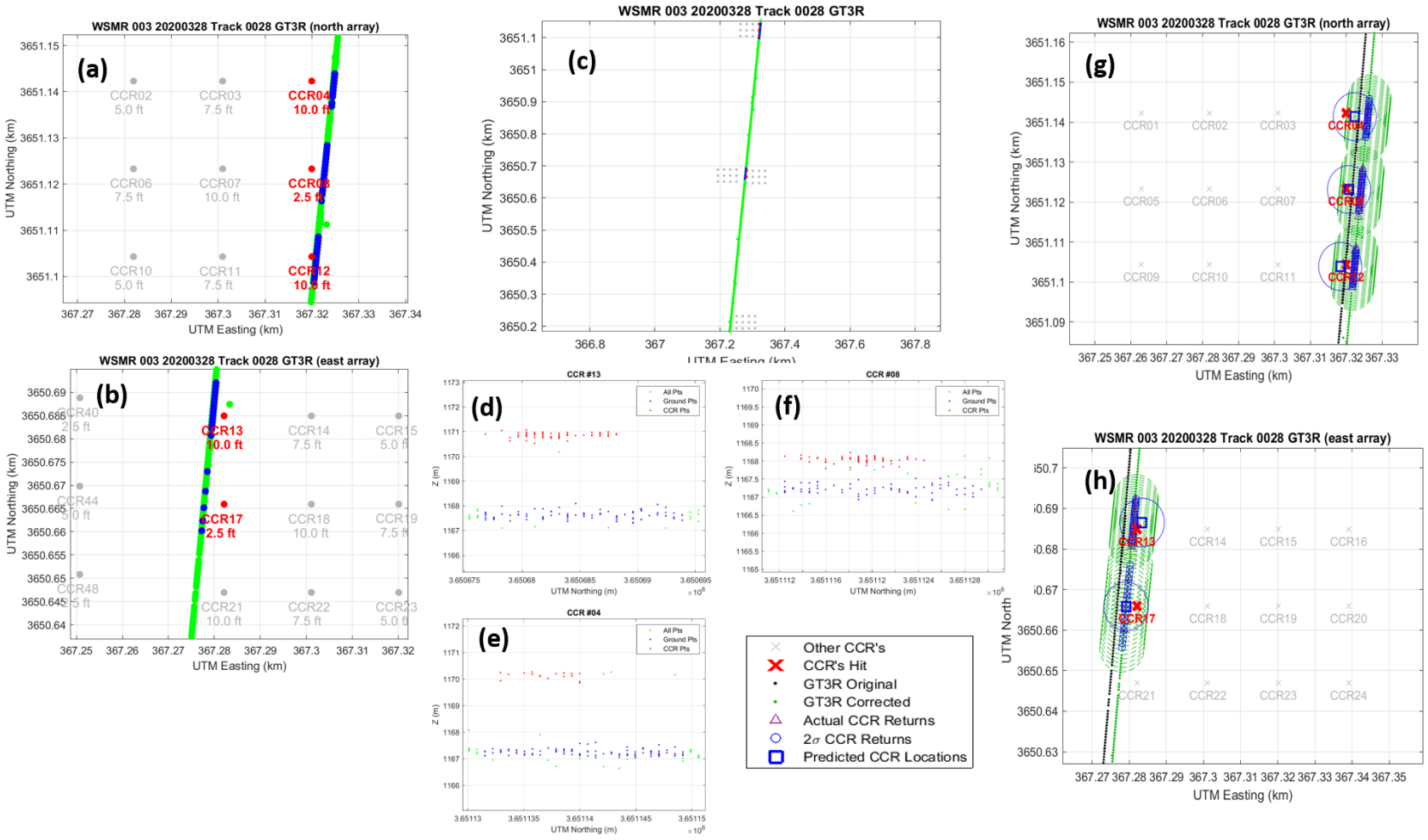

Figure 1. Signal analysis for WSMR overpass on 28 March 2020 where the laser illuminated 5 CCRs within one descending ground track; 3 of the illuminated CCRs were in the north array and 2 were in the east. Plots (a-c) show the ATL03 surface signal in green and the ATL03 CCR signal in blue. Plots (d-f) provide the returns from CCR04, 08 and 12 in the north array indicating the height of each CCR relative to the surface. Plots (g-h) show the estimated chord lengths (blue) and the solution (green) for determination of the footprint diameter and geolocation offsets that correspond to the geometry of the known locations of the illuminated optical components.

249

WSMR overpass date	Beam Ground-track	Beam strength	Off-nadir angle (deg)	Slant range (m)	ATLAS spot number	Local time of collection	Horizontal geolocation error (m)	Footprint diameter (m)
3/31/2019	GT2R	Weak	2.46	485162	4	08:37	2.5	10.6
5/31/2019	GT2R	Weak	0.37	484743	4	17:04	3.0	8.5
9/28/2019	GT2R	Strong	2.52	485037	3	11:56	5.0	12.0
10/12/2019	GT2R	Strong	4.87	486609	3	23:15	3.8	10.6
10/31/2019	GT2R	Strong	3.27	484847	3	10:24	2.8	11.4
1/07/2020	GT1R	Strong	3.22	485483	5	18:03	0.7	8.3
2/08/2020	GT3R	Strong	1.67	484471	1	16:31	7.7	11.6
3/28/2020	GT3R	Strong	4.06	485998	1	03:16	4.3	12.0
5/09/2020	GT3R	Strong	1.72	484482	1	13:11	2.1	10.0
Average WSMR geolocation error and beam diameter							3.5 ± 1.9	10.6 ± 1.3
88S overpass date	**Beam Ground-track**	**Beam strength**	**Off-nadir angle (deg)**	**Slant range (m)**	**ATLAS spot number**	**Local time of collection**	**Horizontal geolocation error (m)**	**Footprint diameter (m)**
12/10/2018	GT2R	Strong	-	511475	3	21:49	0.4	11.6
1/18/2019	GT3L	Strong	-	511930	5	19:17	2.4	9.8
11/27/2019	GT3L	Weak	2.78	512538	2	04:27	3.3	11.1
12/30/2019	GT3R	Strong	2.81	512031	1	02:55	2.0	12.4
1/13/2020	GT2R	Strong	0.67	511625	3	04:47	8.5	11.5
1/24/2020	GT3R	Strong	2.81	512554	1	22:31	3.8	11.5
Average 88S geolocation error and beam diameter							3.4 ± 2.5	11.3 ± 0.8

250

4. Discussion

The overpass summary for on-orbit performance of ICESat-2 serves as evidence of the mission meeting both the requirement for geolocation accuracy and the pointing control capability. Table 1 provides the results of each relevant case at WSMR and 88S. Aggregation of the results give an average footprint diameter of 10.9 m with a standard deviation of 1.2 m and a median value of 11.4 m. The horizontal geolocation error, overall, is 3.5 m ± 2.1 m. Results specific to WSMR indicate the diameter retrievals are fairly consistent over the 9 cases within a range of 8.3 m to 12 m (average value 10.6 m ±1.3 m). Using the 6 overpass cases for 88S independent of WSMR determines an average diameter of 11.3 m ±0.8 m. The pre-launch measurements of the ATLAS laser beam divergence were 21.4 μrad and 19.7 μrad for the semi-major and semi-minor axes respectively (A. Martino, pers, comm.). Using these pre-launch measurements and the orbital altitude range of ICESat-2 (486 km – 512 km) yields 9.5 m/10.4 m – 10.0 m/10.9 m for the semi-major and semi-minor axes of the laser spots on the surface, in good agreement with our observations.

To understand more completely the variability in footprint diameter retrievals we evaluated parameters that might influence the footprint characteristics at the surface. Figure 2 provides a summary of the correlation or lack of correlation between the footprint diameter values and these parameters investigated and is discussed in the subsequent sections.

4.1 Satellite Altitude

Since the ICESat-2 orbit is nearly frozen, the satellite altitude has a dependence on latitude. Although the altitude at WSMR for each overpass are ~484 km, the slant range associated with the off-nadir pointing angle (Table 1) creates a longer divergence path length. However, the largest off pointing angle theoretically increases the spot size by only 5 cm relative to the nadir. The average altitude at 88S is nearly 30 km higher than at WSMR which would implies that the spot would be larger by ~1 m if solely based on path length. The 0.7 m average diameter difference between the two sites' altitudes is consistent with this expected variation but does not account the potential impact of diameter retrieval relative to along-track alignments with the major or minor axes. The lower variability in diameter values at 88S in comparison to that at WSMR could be attributed to the consistency of the collection parameters (altitude and path length) or the lower susceptibility to atmospheric influence based on the reduced vertical height of the boundary layers

and the low water vapor content in this region. The relationship between the diameter retrievals and slant range is provided in Figure 2(d) for all cases.

4.2 Atmospheric Parameters

The atmospheric parameters examined are based on the GEOS-FPIT model results used to calculate the wet and dry tropospheric correction to ATL03 photon heights (Palm et al., 2019). Figure 2(a-c) shows column properties comparison for two specific cases at WSMR, while Figure 2(e-f) make similar column-property comparisons between all of the passes at both WSMR and 88S.

Humidity. The relative humidity (RH) and specific humidity (SH) profiles for WSMR in Figures 2(a-b) indicate large amounts of moisture in the lower atmosphere for the 31 May 2019 (8.5 m diameter) case, where SH is > 2 times larger than for the 28 March 2020 (12.0 m diameter) case at 4 km above the surface. Overall, at WSMR, the decrease in diameter with increasing SH confirms that moisture content has a negative effect on detecting surface signal. Footprint diameters for WSMR and 88S are shown with respect to the total SH and RH in Figure 2(f). RH and SH are used here to indicate the amount of water vapor present in the lowest portion of the atmosphere. Figure 2(f) indicates that RH is high throughout the column, but these results are misleading due to the cold temperatures at 88S, which are < -23 °C near the surface for all cases. The average temperature at WSMR near the surface was 13.4 °C. Because of this 36 °C difference, the 88S specific humidity is an order of magnitude lower than at WSMR. Overall, SH for the cases at 88S are nearly the same across each instance regardless of apparent footprint diameter determined with the CCR method and thus do not indicate moisture is having an effect on surface signal at this location.

Optical Depth. The column optical depth comparison for the May 2019/March 2020 results at WSMR in Figure 2(c) indicates a correlation between increasing optical depth and smaller diameters due to increasing attenuation. Initially, the column optical depth was analyzed to determine the presence of cloud and aerosol layers as the most probable parameter for indicating signal attenuation. However, the ATL09 CAB and related parameters capture only limited information on the state of the atmosphere at a given location. Clouds above the 12 km threshold are typically not detected and increased moisture in the lower atmosphere is also not well detected. With increased moisture content, the possibility of additional aerosols not observed by the satellite

311 increases as well. Looking over all WSMR cases in Table I, Figure 2(e) indicates that the primary
312 range of optical depths is between 0.05 – 1.05, although there are several cases that exceed 1.05.
313 It is fitting that the cases with the largest diameters have the lowest optical depths, but there is not
314 a clear statistical relationship determined. For the 88S CCRs, the column optical depth is high for
315 the lowest diameter case but remains low to moderate for the other cases. There is potential for
316 optical depth to be useful at 88S due to a lower tropospheric height (i.e., below the ICESat-2
317 threshold) and lack of water vapor in the atmosphere, but there is no apparent trend within this
318 small sample.

319 *Atmospheric Parameter Summary*. The trends described, although based on an overall
320 small amount of data, suggest that moisture content is inversely related to the footprint diameter
321 for mid-latitude locations, where the moisture content values are more significant than in the polar
322 regions. Increased moisture could indicate that there is also an increase in forward scattering that
323 widens the full laser footprint at the surface but lowers the detected energy, relative to clear
324 atmosphere. That is, the scattering creates a higher probability that the signal photons on the outer
325 edges of a widened footprint are mistaken for noise or are further scattered. While the connection
326 with atmospheric moisture content at 88S is not apparent, another potential cause of low-level
327 attenuation at 88S is blowing snow in the near-surface layer. Blowing snow acts similarly to an
328 aerosol layer, where the small ice crystals provide both forward scattering and backscattering on
329 the laser energy. Although not shown, the case with the lowest diameter had a moderate blowing
330 snow identified in ATL09, but several of the other 'normal' diameter cases also had at least
331 moderate blowing snow detected. Additional data collection in the coming Austral summer might
332 help with a more in depth understanding of the relationship between ICESat-2 footprint diameters
333 and both blowing snow and optical depth.

334

335 ### 4.3 Seasonality of Returns from 88S

336 We note that we only received returns from the Antarctic CCRs during the austral summer
337 months (late November through late January) despite nominal pointing control throughout the
338 calendar year. While it is possible that individual attempts at pointing to a CCR array could be
339 compromised by blowing snow or a snowfall event that attenuates the laser returns, this seems like
340 an unlikely explanation for the total lack of CCR returns over the Feb – November months. We

note that the surface reflections during this time period were nominal (Brunt et al., 2019)and suggest that the lack of CCR returns in the Austral winter is due to frost build up on either the optical glass or the plastic cap that holds the optical glass due to near-surface atmospheric supersaturation. This could be tested by relative humidity measurements at the CCR sites, or mitigated by heating the CCRs during satellite overpasses, but we acknowledge the difficulty of making humidity measurements at such low ambient temperatures. CCR signatures are recovered shortly after the sun rises at this latitude, suggesting a thermodynamic explanation.

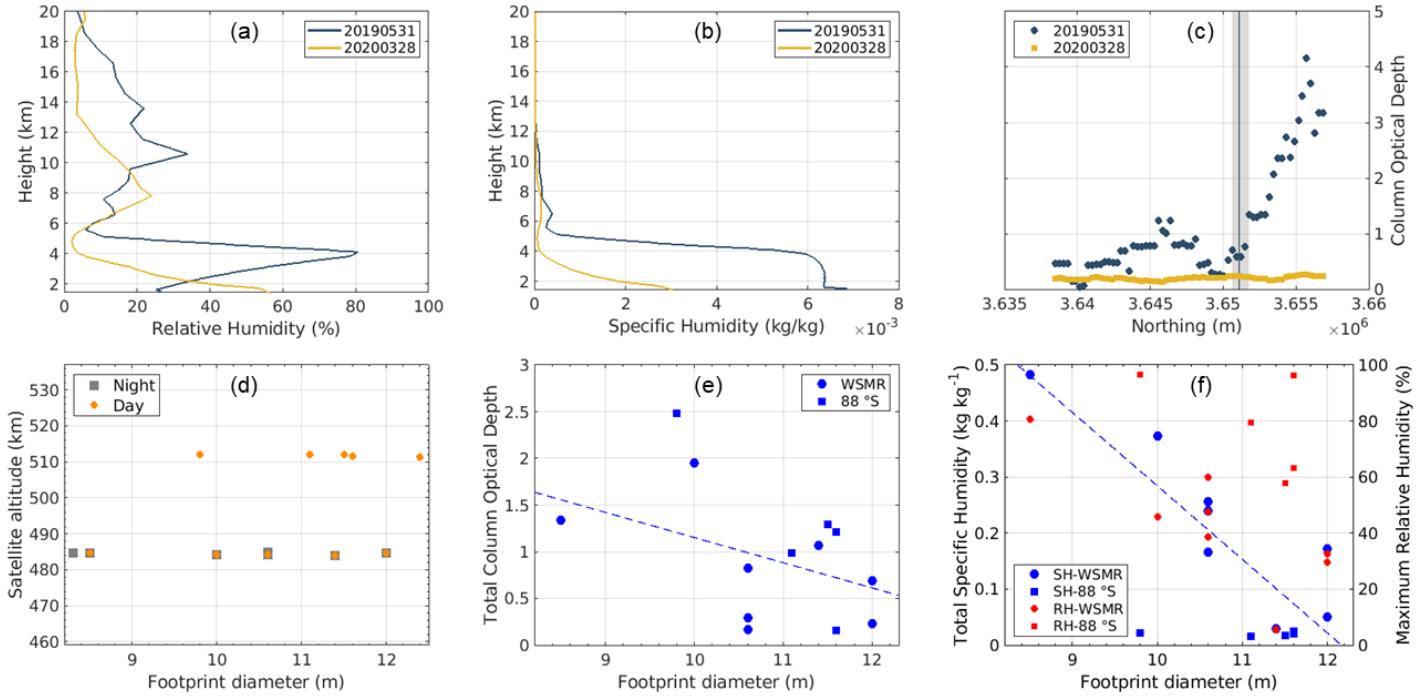

Figure 2. Comparisons of relative humidity (RH) profiles, specific humidity (SH) profiles, and column optical depth are provided in (a), (b), and (c), respectively, for the 31 May 2019 (8.5 m diameter) and 28 March 2020 (12.0 m diameter) WSMR cases. The line and gray shading in (c) mark the location of the CCRs. In (d), footprint diameter is evaluated with the satellite altitude for WSMR and 88S. Day and night designation is provided as well. Panel (e) show the column optical depth and panel (f) shows the total SH and maximum RH in the lower atmosphere with respect to footprint diameter for WSMR (blue circles) and 88S (blue squares). The dashed line in (f) is the best-fit for WSMR cases only.

6. Summary

We have shown that the passive method of CCR signature analysis provides an assessing and monitoring capability for geolocation validation of space-based laser altimetry. The results from two validation sites indicate that ICESat-2 geolocated photons are accurate to within the mission requirement of 6.5 m. The methodology also provides an assessment of the effect laser spot diameter. To date, the successful satellite overpasses of the sites conclude that the diameter of the ATLAS footprint is 10.9 m ±1.3 m. The variation in independent diameter value retrievals is associated with spacecraft altitude, atmospheric attenuation that can be correlated to optical depth and humidity, or moisture levels.

Acknowledgments and Data Availability

The authors wish to thank the ICESat-2 Project Science Office for the support under NASA grant NNX15AC68G. We thank the three 88S Traverse teams, the NSF Office of Polar Programs, and the numerous personnel with the U.S. Antarctic Program for supporting the deployment of the Antarctic CCR arrays. Special thanks to colleagues at the Antarctic Meteorological Research Center for discussions on the potential for CCR frost build up. Data used in this study is compliant with FAIR data standards and publically available/archived at National Snow and Ice Data Center: doi: https://doi.org/10.5067/ATLAS/ATL03.003

References

Brunt, K. M., Neumann, T. A. and Smith, B. E. (2019), Assessment of ICESat-2 ice-sheet surface heights, based on comparisons over the interior of the Antarctic ice sheet. Geophysical Research Letters, 46(22), 13,072-13,078, doi:10.1029/2019GL084886.

Luthcke, S.B, Pennington, T., Rebold, T., and Thomas, T. (2019), Algorithm Theoretical Basis Document (ATBD) for ATL03g ICESat-2 Receive Photon Geolocation, ICESat-2 Scientific Computing Facility, https://icesat-2.gsfc.nasa.gov/sites/default/files/page_files/ICESat2_ATL03g_ATBD_r002.pdf

Magruder, L. A., and K. M. Brunt (2018), Performance analysis of airborne photon-counting lidar data in preparation for the ICESat-2 mission, IEEE Trans. Geosci. and Rem. Sensing, 56, 2911-2918, doi: 10.1109/TGRS.2017.2786659.

Magruder, L., K. Brunt and M. Alonzo (2020a), Horizontal geolocation validation for ICESat-2 with corner-cube retroreflectors, Remote Sensing, in revision.

Magruder, L., T. Neumann and N. Kurtz (2020b), Overview of the ICESat-2 mission, Geophysical Research Letters, in review.

Markus, T., and Coauthors (2017), The Ice, Cloud, and land Elevation Satellite-2 (ICESat-2): Science requirements, concept, and implementation, Rem. Sens. of Env., 190, 260-273, doi: 10.1016/j.rse.2016.12.029.

Martino, A.J., Neumann, T.A., Kurtz, N.T. and McLennan, D. (2019) ICESat-2 mission overview and early performance, Proc. SPIE 11151, Sensors, Systems and Next-Generation Satellites XXIII, 111510C; https://doi.org/10.1117/12534938.

Neuenschwander, A., and K. Pitts (2019), The ATL08 land and vegetation product for the ICESat-2 mission, Rem. Sens. of Env., 221, 247-259, doi: 10.1016/j.rse.2018.11.005.

Neumann, T.A., and Co-Authors (2019a), The Ice, Cloud and Land Elevation Satellite-2 mission: A global geolocated photon product derived from the Advanced Topographic Laser Altimeter System, Remote Sens. Of Env., 233, doi: 10.106/j.rse.2019.111325.

Neumann, T. A., A. Brenner, D. Hancock, J. Robbins, J. Saba, K. Harbeck, A. Gibbons, J. Lee, S. B. Luthcke, T. Rebold, et al. (2019b). *ATLAS/ICESat-2 L2A Global Geolocated Photon Data, Version 3*. Boulder, Colorado USA. NASA National Snow and Ice Data Center Distributed Active Archive Center. doi: https://doi.org/10.5067/ATLAS/ATL03.003. [May 2020]

Palm, S., Yang, Y., & Herzfeld, U. (2020). Algorithm Theoretical Basis Document (ATBD) for the atmosphere, Part I: Level 2 and 3 data products. ICESat-2 Data Products, https://icesat-2.gsfc.nasa.gov/science/data-products.

Rogers, R. R., and M. K. Yau (1996), A Short Course in Cloud Physics. Butterworth-Heinemann publishers, pp. 304.

Smith, B. (2018), Algorithm Theoretical Basis Document (ATBD) for land ice along-track height product (ATL06), ICESat-2 Scientific Computing Facility, https://icesat-2-scf.gsfc.nasa.gov/atbd_docs.

Schutz, B. E., H. J. Zwally, C. A. Shuman, D. Hancock, and J. P. DiMarzio (2005), Overview of the ICESat mission, Geophys. Res. Lett., 32, L21S01, doi: 10.1029/2005GL024009.

Sun, X., Smith, D.E., Hoffman, E.D., Wake, S.W., Cremons, D.R., Mazarico, E., Lauenstein, J., Zuber, M.T., and Aaron, E.C. (2019) Small and lightweight laser retro-reflector arrays for lunar landers, Applied Optics, Vol. 58, No. 33, doi: 10.1364/AO.58.009259